Appl. Math. Mech. -Engl. Ed., **37**(3), 303–314 (2016)
DOI 10.1007/s10483-015-2007-6

Applied Mathematics and Mechanics (English Edition)

Pull-in instability analyses for NEMS actuators with quartic shape approximation*

Junsheng DUAN[1,†], Zongxue LI[2], Jinyuan LIU[3]

1. School of Sciences, Shanghai Institute of Technology, Shanghai 201418, China;
2. College of Computer and Information, Inner Mongolia Medical University, Hohhot 010110, China;
3. Department of Information Management, Party School of the Inner Mongolia Committee of the Communist Party of China, Hohhot 010070, China

Abstract The pull-in instability of a cantilever nano-actuator model incorporating the effects of the surface, the fringing field, and the Casimir attraction force is investigated. A new quartic polynomial is proposed as the shape function of the beam during the deflection, satisfying all of the four boundary values. The Gaussian quadrature rule is used to treat the involved integrations, and the design parameters are preserved in the evaluated formulas. The analytic expressions are derived for the tip deflection and pull-in parameters of the cantilever beam. The micro-electromechanical system (MEMS) cantilever actuators and freestanding nano-actuators are considered as two special cases. It is proved that the proposed method is convenient for the analyses of the effects of the surface, the Casimir force, and the fringing field on the pull-in parameters.

Key words micro-electromechanical system (MEMS), nano-electromechanical system (NEMS), Casimir force, pull-in instability, quartic shape function

Chinese Library Classification O302, O39, O241.4
2010 Mathematics Subject Classification 34B15, 65Z99, 81T55

1 Introduction

Beam-type electrostatic actuators are common components for the construction of micro-electromechanical systems (MEMSs) and nano-electromechanical systems (NEMSs)[1]. A cantilever MEMS/NEMS actuator is composed of a cantilever beam of the length L with a uniform rectangular cross section of the width w and the thickness h, which is suspended over a conductive substrate and separated by a dielectric spacer (see Fig. 1).

A voltage difference between the two electrodes causes the upper movable electrode to deflect towards the fixed ground electrode. At a critical voltage, the movable electrode becomes unstable, and collapses onto the ground electrode. The voltage and deflection of the actuator at this critical state are used to designate the pull-in parameters[2].

* Received Jan. 9, 2015 / Revised Apr. 18, 2015
Project supported by the National Natural Science Foundation of China (No. 11201308), the Natural Science Foundation of Shanghai (No. 14ZR1440800), and the Innovation Program of the Shanghai Municipal Education Commission (No. 14ZZ161)
† Corresponding author, E-mail: duanjs@sit.edu.cn

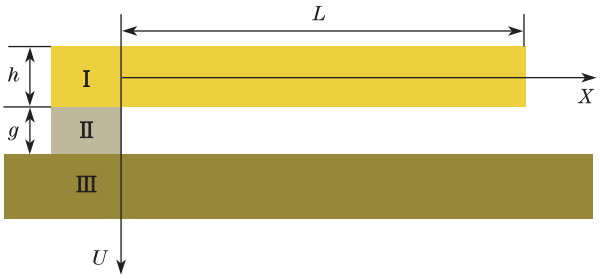

Fig. 1 Schematic representation of cantilever actuator: I cantilever beam; II dielectric spacer; III fixed ground electrode

The pull-in behavior and parametric analyses of MEMS/NEMS actuators have been widely studied by many authors[2–18]. For NEMS actuators, the effects of the intermolecular forces[19–22] such as the van der Waals force and the Casimir force are always considered.

The distributed parameter model of the deflection of nano-beams constitutes a boundary value problem for a non-linear fourth-order ordinary differential equation. Lin and Zhao[16] and Guo and Zhao[23] studied the dynamic behavior of nano-scale electrostatic actuators by considering the effect of the van der Waals force. Guo and Zhao[24] and Lin and Zhao[25] investigated the influence of the van der Waals force and the Casimir force on the stability of the electrostatic torsional NEMS actuators. Abadyan et al.[9], Koochi et al.[5,13], Noghrehabadi et al.[14], and Duan et al.[26] used the Adomian decomposition method to treat similar models of non-linear boundary value problems. Ma et al.[17] studied the instability of cantilever NEMS actuators by the homotopy perturbation method. Ramezani et al.[6,15] and Duan and Rach[18] investigated the instability of nano-cantilevers with the assumption of a second-degree polynomial as the shape function of the beam during the deflection.

Surface energy effects are very important in modeling a nano-scale structure due to the large surface area/volume ratio of the structure. Surface effects play a crucial role in the pull-in performance of nano-actuators. Gurtin and Murdoch[27] developed a continuum theory to model both the residual surface stress and the surface elasticity to investigate the surface effects on the elastic behavior of beam-type nano-structures[28–30], where the Casimir attraction and fringing field effects were neglected.

In this paper, we consider the distributed parameter model of the NEMS cantilever actuators, incorporating the effects of the surface energy, the Casimir force, and the fringing field, and investigate the pull-in parameters. A new shape function is used for the beam during the deflection. In Section 2, we establish the model as a boundary value problem for a non-linear fourth-order ordinary differential equation. Our main results are presented in Section 3, where a quartic shape function of the beam during the deflection is proposed, satisfying all of the four boundary values. The Gaussian quadrature rule is used to treat the involved integrations, retaining the designed parameters in the evaluated formulas. Section 4 summarizes our conclusions.

2 Distributed parameter model

The governing equation for the distributed parameter model based on the Euler-Bernoulli beam assumptions can be written as follows[5–6]:

$$(EI)_{\text{eff}}\frac{\mathrm{d}^4U}{\mathrm{d}X^4} = F_{\text{s}} + F_{\text{elec}} + F_{\text{cas}}, \tag{1}$$

where U is the transverse deflection of the beam as measured from its axis towards the surface of the fixed ground electrode, X is the position along the axis of the beam as measured from

the clamped end, $(EI)_{\text{eff}}$ is the effective bending rigidity of the beam incorporating the surface elasticity effect, and F_{s}, F_{elec}, and F_{cas} are the distributed transverse forces resulting from the surface effect, the electrostatic force, and the Casimir force per unit length of the beam, respectively.

Based on the composite beam theory and the assumption that the thickness of the surface layer is much smaller than the beam thickness h, the effective bending rigidity $(EI)_{\text{eff}}$ for a beam with a rectangular cross section can be derived as follows:

$$(EI)_{\text{eff}} = EI + \frac{1}{2}E^{\text{s}}wh^2,$$

where E is the corresponding elastic modulus of the material, I is the area moment of the inertia of the cross section of the beam, i.e., $I = wh^3/12$, and E^{s} is the surface elastic modulus[28–29,31–32]. The distributed transverse force resulting from the surface effect is[28–29,32]

$$F_{\text{s}} = 2\tau^0 w\frac{\mathrm{d}^2U}{\mathrm{d}X^2}, \tag{2}$$

where τ^0 is the residual surface stress along the beam longitudinal direction. The first-order fringing field correction of the electrostatic force per unit length of the beam is[33–34]

$$F_{\text{elec}} = \frac{\varepsilon_0 wV^2}{2(g-U)^2}\Big(1+\frac{0.65(g-U)}{w}\Big), \tag{3}$$

where ε_0 is the vacuum permittivity expressed by

$$\varepsilon_0 = 8.854\times10^{-12}\,\text{C}^2\cdot\text{N}^{-1}\cdot\text{m}^{-2},$$

V is the applied voltage, and g is the original gap between the two electrodes when there is no deflection. The Casimir force per unit length of the beam is[5,14,21]

$$F_{\text{cas}} = \frac{\pi^2\hbar vw}{240(g-U)^4}, \tag{4}$$

where $\hbar$ is the reduced Planck's constant, and v is the speed of light, which are

$$\hbar = 1.055\times10^{-34}\,\text{J}\cdot\text{s}, \quad v = 2.998\times10^{8}\,\text{m}\cdot\text{s}^{-1}.$$

Substituting Eqs. (2), (3), and (4) into Eq. (1) and introducing the dimensionless variables $u = U/g$ and $x = X/L$, we can transform the governing equation into the dimensionless form as follows:

$$\frac{\mathrm{d}^4u}{\mathrm{d}x^4} = \eta\frac{\mathrm{d}^2u}{\mathrm{d}x^2} + \frac{\alpha}{(1-u(x))^4} + \frac{\beta}{(1-u(x))^2} + \frac{\gamma\beta}{1-u(x)}, \quad 0<x<1, \tag{5}$$

where

$$\eta = \frac{2\,\tau^0 wL^2}{(EI)_{\text{eff}}}, \quad \alpha = \frac{\pi^2\hbar vwL^4}{240g^5(EI)_{\text{eff}}}, \quad \beta = \frac{\varepsilon_0 wV^2L^4}{2g^3(EI)_{\text{eff}}}, \quad \gamma = \frac{0.65g}{w}. \tag{6}$$

In the above equations, η, α, β, and γ are the surface energy parameter, the intermolecular Casimir force parameter, the electrostatic force parameter, and the fringing field parameter, respectively. They can characterize the magnitudes of the responding forces. These parameters are within their variation ranges[8]. The surface energy parameter η can be negative. $\eta = 0$, $\alpha = 0$, and $\beta = 0$ correspond to the cases of free-surface-energy nano-actuators, MEMS microactuators, and freestanding nano-actuators, respectively.

For the cantilever NEMS, the boundary conditions are

$$u(0)=0,\quad u'(0)=0,\quad u''(1)=0,\quad u'''(1)=0. \tag{7}$$

We denote the maximum cantilever tip deflection as $u_{\rm tip}=u(1)$, and investigate the pull-in parameters $u_{\rm tip}^{\rm PI}$ and $\beta^{\rm PI}$. From the third equality in Eq. (6), the pull-in voltage $V^{\rm PI}$ can be characterized in terms of the pull-in parameter $\beta^{\rm PI}$ as follows:

$$V^{\rm PI}=\sqrt{2\,g^3(EI)_{\rm eff}\,\beta^{\rm PI}/(\varepsilon_0 wL^4)}.$$

3 Quartic shape function and pull-in parameters

First, we convert Eqs. (5)–(7) into an equivalent non-linear integral equation[35] so as to determine all of the integration constants in terms of the boundary conditions. Secondly, we rewrite Eq. (5) in its operator form as follows:

$$\mathcal{L}^4u(x)=\eta\mathcal{L}^2u(x)+\mathcal{N}u(x), \tag{8}$$

where

$$\begin{cases}\mathcal{L}^4(\cdot)=\dfrac{{\rm d}^4}{{\rm d}x^4}(\cdot),\quad \mathcal{L}^2(\cdot)=\dfrac{{\rm d}^2}{{\rm d}x^2}(\cdot),\\[2ex] \mathcal{N}u(x)=\dfrac{\alpha}{(1-u(x))^4}+\dfrac{\beta}{(1-u(x))^2}+\dfrac{\gamma\beta}{1-u(x)}.\end{cases} \tag{9}$$

Introducing the definite integral operators $\mathcal{L}_0^{-2}(\cdot)$ and $\mathcal{L}_1^{-2}(\cdot)$ as follows:

$$\mathcal{L}_0^{-2}f(x)=\int_0^x\int_0^x f(\tau){\rm d}\tau{\rm d}x=\int_0^x(x-\tau)f(\tau){\rm d}\tau, \tag{10}$$

$$\mathcal{L}_1^{-2}f(x)=\int_1^x\int_1^x f(\tau){\rm d}\tau{\rm d}x=\int_x^1(\tau-x)f(\tau){\rm d}\tau, \tag{11}$$

where the iterated integrals can be rewritten as the respective simple integrals by exchanging the integration order, we have

$$\begin{aligned}\mathcal{L}_0^{-2}\mathcal{L}_1^{-2}\mathcal{L}^4u(x)\ &=u(x)-\Phi(x)\\ &=u(x)-u(0)-xu'(0)-\frac{x^2}{2}u''(1)-\Big(\frac{x^3}{6}-\frac{x^2}{2}\Big)u'''(1).\end{aligned}$$

Substituting the boundary conditions in Eq. (7), we have $\Phi(x)=0$. Hence, applying the operator $\mathcal{L}_0^{-2}\mathcal{L}_1^{-2}(\cdot)$ on both sides of Eq. (8) yields the equivalent non-linear Volterra integral equation as follows:

$$u(x)=\eta\mathcal{L}_0^{-2}\mathcal{L}_1^{-2}\mathcal{L}^2u(x)+\mathcal{L}_0^{-2}\mathcal{L}_1^{-2}\mathcal{N}u(x), \tag{12}$$

in which all of the boundary conditions have been incorporated. Setting $x=1$ and denoting $u(1)=u_{\rm tip}$, we obtain

$$u_{\rm tip}=\eta(\mathcal{L}_0^{-2}\mathcal{L}_1^{-2}\mathcal{L}^2u(x))_{x=1}+(\mathcal{L}_0^{-2}\mathcal{L}_1^{-2}\mathcal{N}u(x))_{x=1}. \tag{13}$$

To analyze the deflection and pull-in parameters of the cantilever beam, some authors proposed the following second-degree function to approximate the beam deflection[6,15,18,36–37]:

$$u(x)=u_{\rm tip}x^2, \tag{14}$$

which satisfies the boundary conditions

$$u(0)=0,\quad u'(0)=0,\quad u'''(1)=0,$$

but does not satisfy the remaining boundary condition $u''(1)=0$. This means that the curvature at the free end should be zero.

Here, we present a new approximation of the beam by the quartic function

$$u(x)=u_{\text{tip}}\Big(2x^2-\frac{4x^3}{3}+\frac{x^4}{3}\Big). \tag{15}$$

We observe that this new approximation satisfies all of the four boundary values in Eq. (7) by examining the first- and second-order derivatives, respectively, i.e.,

$$u'(x)=\frac{4}{3}u_{\text{tip}}x(3-3x+x^2)>0,\quad u''(x)=4u_{\text{tip}}(x-1)^2>0,$$

where $0<x<1$. The quartic shape function in Eq. (12) is a strictly increasing monotone and convex function over the interval $[0,1]$ just as the quadratic shape function in Eq. (14).

Substituting $u(x)=0$ into the right-hand side of Eq. (12), we can obtain the approximation of the beam as follows:

$$u(x)=\frac{\alpha+\beta+\gamma\beta}{8}\Big(2x^2-\frac{4x^3}{3}+\frac{x^4}{3}\Big).$$

It is in the form of Eq. (15). We use the new quartic shape function (15) to analyze the deflection and pull-in parameters of the beam-type cantilever actuators. Substituting Eq. (15) into Eq. (13) yields

$$u_{\text{tip}}=\eta\frac{u_{\text{tip}}}{18}+\int_0^1(1-s)\int_s^1(\tau-s)\mathcal{N}\Big(u_{\text{tip}}\Big(2\tau^2-\frac{4\tau^3}{3}+\frac{\tau^4}{3}\Big)\Big)\mathrm{d}\tau\mathrm{d}s. \tag{16}$$

By exchanging the integration order in Eq. (16) and calculating the integration with respect to the variable s, we obtain

$$u_{\text{tip}}=\eta\frac{u_{\text{tip}}}{18}+\frac{1}{6}\int_0^1(3\tau^2-\tau^3)\mathcal{N}\Big(u_{\text{tip}}\Big(2\tau^2-\frac{4\tau^3}{3}+\frac{\tau^4}{3}\Big)\Big)\mathrm{d}\tau. \tag{17}$$

The integral on the right-hand side of Eq. (17) cannot be analytically calculated by the available computer algebra systems that utilize the Risch algorithm such as MATHEMATICA. We mention that this integral can be exactly and analytically calculated if the second-degree shape function (14) is used. Here, we rely on a numeric integral method. To acquire the superior accuracy of a numeric integral by use of the minor integral nodes, we use the Gaussian quadrature rule. For the relevant details of the Gaussian quadrature rule, see Appendix A[38].

To perform the integration in Eq. (17) by the Gaussian quadrature rule, we use the transformation $\tau=(z+1)/2$ to obtain the canonical form as follows:

$$\frac{16}{3}(18-\eta)u_{\text{tip}}=\int_{-1}^1(5-z)(1+z)^2\mathcal{N}\Big(\frac{u_{\text{tip}}}{48}(1+z)^2(17-6z+z^2)\Big)\mathrm{d}z. \tag{18}$$

Applying the Gaussian quadrature rule, we have

$$\frac{16}{3}(18-\eta)u_{\text{tip}}=\sum_{i=1}^n\omega_i(5-z_i)(1+z_i)^2\mathcal{N}\Big(\frac{u_{\text{tip}}}{48}(1+z_i)^2(17-6z_i+z_i^2)\Big), \tag{19}$$

where n is the number of the integral nodes, z_i are the integral nodes, and ω_i are the weights, which can be readily computed for a specified positive integer n (see Appendix A).

From Eq. (19) and substituting the operator $\mathcal{N}$ into Eq. (9), we can obtain

$$\beta = f_1(u_{\rm tip}, \alpha, \gamma, \eta) = \frac{\dfrac{16}{3}(18-\eta)u_{\rm tip} - \alpha\, g_3(u_{\rm tip})}{g_1(u_{\rm tip}) + \gamma\, g_2(u_{\rm tip})}, \tag{20}$$

where

$$\begin{cases} g_1(u_{\rm tip}) = \displaystyle\sum_{i=1}^{n} \frac{\omega_i(5-z_i)(1+z_i)^2}{\left(1-\frac{u_{\rm tip}}{48}(1+z_i)^2(17-6z_i+z_i^2)\right)^2}, \\ g_2(u_{\rm tip}) = \displaystyle\sum_{i=1}^{n} \frac{\omega_i(5-z_i)(1+z_i)^2}{1-\frac{u_{\rm tip}}{48}(1+z_i)^2(17-6z_i+z_i^2)}, \\ g_3(u_{\rm tip}) = \displaystyle\sum_{i=1}^{n} \frac{\omega_i(5-z_i)(1+z_i)^2}{\left(1-\frac{u_{\rm tip}}{48}(1+z_i)^2(17-6z_i+z_i^2)\right)^4}. \end{cases}$$

For example, we take $n = 5$ and solve for β from Eq. (19). Then, we have

$$\begin{aligned} \beta = {} & \Big(5.333\,33(18-\eta)u_{\rm tip} - \frac{3.524\,28\alpha}{(1-0.937\,455u_{\rm tip})^4} - \frac{5.054\,29\alpha}{(1-0.693\,258u_{\rm tip})^4} \\ & - \frac{2.844\,44\alpha}{(1-0.354\,167u_{\rm tip})^4} - \frac{0.564\,663\alpha}{(1-0.091\,065\,4u_{\rm tip})^4} - \frac{0.012\,317\,2\alpha}{(1-0.004\,265\,09u_{\rm tip})^4}\Big) \\ & \Big/\Big(\frac{3.524\,28}{(1-0.937\,455u_{\rm tip})^2} + \frac{3.524\,28\gamma}{1-0.937\,455u_{\rm tip}} + \frac{5.054\,29}{(1-0.693\,258u_{\rm tip})^2} \\ & + \frac{5.054\,29\gamma}{1-0.693\,258u_{\rm tip}} + \frac{2.844\,44}{(1-0.354\,167u_{\rm tip})^2} + \frac{2.844\,44\gamma}{1-0.354\,167u_{\rm tip}} \\ & + \frac{0.564\,663}{(1-0.091\,065\,4u_{\rm tip})^2} + \frac{0.564\,663\gamma}{1-0.091\,065\,4u_{\rm tip}} + \frac{0.012\,317\,2}{(1-0.004\,265\,09u_{\rm tip})^2} \\ & + \frac{0.012\,317\,2\gamma}{1-0.004\,265\,09u_{\rm tip}}\Big), \end{aligned} \tag{21}$$

which retains all of the designed parameters.

We take $\alpha = 0.4$, $\gamma = 0.6$, and $\eta = 0$ and 2, respectively, and plot the curves of β versus $u_{\rm tip}$ in Fig. 2.

The pull-in parameters $u_{\rm tip}^{\rm PI}$ and $\beta^{\rm PI}$ are determined by

$$\frac{{\rm d}\beta}{{\rm d}u_{\rm tip}} = 0, \tag{22}$$

i.e., when the slope is zero. We note that, although we have the applied numeric integration with respect to x, all of the designed parameters are preserved, e.g., the designed parameters in Eq. (21). The result is an analytic expression of parameters, and is applicable to the parametric analyses.

Equation (22) determines the pull-in parameter $u_{\rm tip}^{\rm PI}$. We next replace $u_{\rm tip}$ by $u_{\rm tip}^{\rm PI}$ and rewrite Eq. (22) as follows:

$$f_2(u_{\rm tip}^{\rm PI}, \alpha, \gamma, \eta) = 0. \tag{23}$$

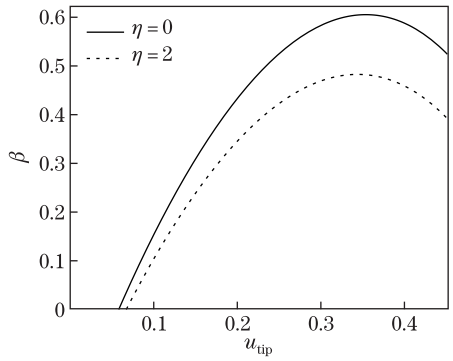

Fig. 2 Curves of β versus $u_{\rm tip}$ for $\alpha = 0.4$, $\gamma = 0.6$, and $\eta = 0$, 2

From Eq. (20), we have

$$\Big(\frac{16}{3}(18-\eta) - \alpha g_3'(u_{\rm tip}^{\rm PI})\Big)(g_1(u_{\rm tip}^{\rm PI}) + \gamma g_2(u_{\rm tip}^{\rm PI})) - \Big(\frac{16}{3}(18-\eta)u_{\rm tip}^{\rm PI} - \alpha g_3(u_{\rm tip}^{\rm PI})\Big)(g_1'(u_{\rm tip}^{\rm PI}) + \gamma g_2'(u_{\rm tip}^{\rm PI})) = 0, \tag{24}$$

from which we can solve for any of the designed parameters, including the Casimir force parameter α, the fringing field parameter γ, and the surface energy parameter η. Using the pull-in parameter $u_{\rm tip}^{\rm PI}$, we can calculate the pull-in parameter $\beta^{\rm PI}$ by virtue of Eq. (20) as follows:

$$\beta^{\rm PI} = f_1(u_{\rm tip}^{\rm PI}, \alpha, \gamma, \eta). \tag{25}$$

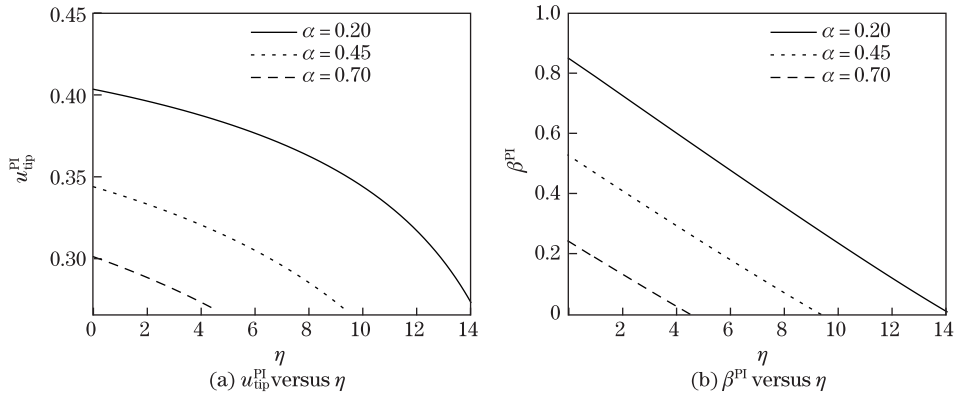

Fig. 3 Curves of $u_{\rm tip}^{\rm PI}$ and $\beta^{\rm PI}$ versus η for $\gamma = 0.65$ and various α

From Eq. (23), we can analyze the effects of α, γ, and η on $u_{\rm tip}^{\rm PI}$. From Eq. (25), we can consider the relation between $\beta^{\rm PI}$ and α, γ, or η.

To achieve higher accuracy, we take ten integral nodes, i.e., $n = 10$, to apply the Gaussian quadrature rule on Eq. (19) in the sequel. We remark that increasing the number of the integral nodes does not cause any technical difficulty, but only adds some additional calculation work.

For the specified values of $\alpha = 0.2$ and $\gamma = 0.65$, $\alpha = 0.45$ and $\gamma = 0.65$, and $\alpha = 0.7$ and $\gamma = 0.65$, we plot the curves of $u_{\rm tip}^{\rm PI}$ and $\beta^{\rm PI}$ versus η by use of Eqs. (23) and (25) (see Fig. 3).

It is shown that $u_{\rm tip}^{\rm PI}$ decreases monotonically and $\beta^{\rm PI}$ decreases when η increases. Moreover, $u_{\rm tip}^{\rm PI}$ and $\beta^{\rm PI}$ decrease when α increases, which is consistent with the results in Refs. [5] and [6].

Through Eqs. (23) and (25), we can obtain the numeric values of $u_{\rm tip}^{\rm PI}$ and $\beta^{\rm PI}$ for different η. The obtained results are listed in Tables 1–3. From the tables, we can see that $\beta^{\rm PI}$ decreases non-linearly as η increases, which means that the curves in Fig. 3(b) are not straight, but are slightly concave.

Table 1 Pull-in parameters for different η when $\alpha = 0.2$ and $\gamma = 0.65$

η	0	1	2	3	4	5	6	7
$u_{\rm tip}^{\rm PI}$	0.403 135	0.399 691	0.395 923	0.391 779	0.387 195	0.382 091	0.376 367	0.369 889
$\beta^{\rm PI}$	0.851 532	0.788 599	0.725 834	0.663 263	0.600 914	0.538 824	0.477 039	0.415 616
η	8	9	10	11	12	13	14	
$u_{\rm tip}^{\rm PI}$	0.362 483	0.353 913	0.343 844	0.331 792	0.317 016	0.298 312	0.273 547	
$\beta^{\rm PI}$	0.354 630	0.294 178	0.234 394	0.175 464	0.117 655	0.061 383	0.007 326	

Table 2 Pull-in parameters for different η when $\alpha = 0.45$ and $\gamma = 0.65$

η	0	1	2	3	4	5	6	7	8	9
$u_{\rm tip}^{\rm PI}$	0.343 844	0.338 769	0.333 249	0.327 216	0.320 587	0.313 255	0.305 088	0.295 913	0.285 502	0.273 547
$\beta^{\rm PI}$	0.527 387	0.468 189	0.409 414	0.351 119	0.293 369	0.236 248	0.179 854	0.124 314	0.069 788	0.016 483

Table 3 Pull-in parameters for different η when $\alpha = 0.7$ and $\gamma = 0.65$

η	0.0	0.5	1	1.5	2	2.5	3	3.5	4.0
$u_{\rm tip}^{\rm PI}$	0.301 291	0.298312	0.295 213	0.291 985	0.288 619	0.285 104	0.281 429	0.277 581	0.273 547
$\beta^{\rm PI}$	0.242 571	0.214 840	0.187 264	0.159 852	0.132 615	0.105 563	0.078 708	0.052 062	0.025 640

Next, we consider two typical special cases.

Case 1 Electrostatic microactuators

Neglecting the intermolecular forces, i.e., setting $\alpha = 0$, leads to the cantilever actuator model in the MEMS. In this case, from Eqs. (20) and (24), we can obtain the equations as follows:

$$\beta^{\rm PI} = \frac{\frac{16}{3}(18-\eta)u_{\rm tip}^{\rm PI}}{g_1(u_{\rm tip}^{\rm PI}) + \gamma\, g_2(u_{\rm tip}^{\rm PI})}, \tag{26}$$

$$g_1(u_{\rm tip}^{\rm PI}) + \gamma\, g_2(u_{\rm tip}^{\rm PI}) - u_{\rm tip}^{\rm PI}\left(g_1'(u_{\rm tip}^{\rm PI}) + \gamma\, g_2'(u_{\rm tip}^{\rm PI})\right) = 0, \tag{27}$$

from which we can obtain $u_{\rm tip}^{\rm PI}$ and $\beta^{\rm PI}$. From Eqs. (26) and (27), we can conveniently consider the effects of γ on $u_{\rm tip}^{\rm PI}$ and γ and η on $\beta^{\rm PI}$.

Especially, if we neglect the influence of the fringing field and the surface effect, i.e., setting $\gamma = 0$ and $\eta = 0$, we can obtain the pull-in parameters as follows:

$$u_{\rm tip}^{\rm PI} = 0.442\,459, \quad \beta^{\rm PI} = 1.670\,160.$$

Case 2 Freestanding nano-actuators

When the nano-actuator becomes freestanding, the voltage difference V between the cantilever beam and the substrate shown in Fig. 1 vanishes. Therefore, the electrostatic force parameter satisfies $\beta = 0$. In this case, from Eq. (20), we have

$$\alpha = \frac{16}{3}(18 - \eta)\frac{u_{\text{tip}}}{g_3(u_{\text{tip}})}. \tag{28}$$

In Fig. 4, we plot the curve of α versus u_{tip} for $\eta = 0$. The critical values of α and u_{tip} are determined by

$$\frac{\mathrm{d}\alpha}{\mathrm{d}u_{\text{tip}}} = \frac{16}{3}(18 - \eta)\frac{g_3(u_{\text{tip}}) - u_{\text{tip}}g_3'(u_{\text{tip}})}{g_3^2(u_{\text{tip}})} = 0. \tag{29}$$

From Eq. (29), we can calculate the critical value u_{tip}^*. Substituting u_{tip}^* into Eq. (28), we can obtain the critical value α^* for $\eta = 0$ as follows:

$$u_{\text{tip}}^* = 0.269\,401, \quad \alpha^* = 0.932\,616.$$

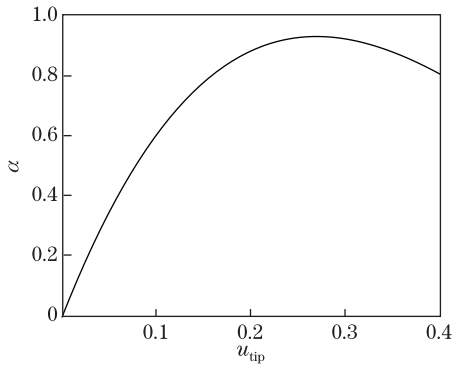

Fig. 4 Curve of α versus u_{tip} for $\eta = 0$

No solution exists when α is greater than the critical value α^*, since the cantilever beam collapses onto the substrate. Therefore, the critical value α^* is considered to be crucial in the cantilever design.

From the second formula in Eq. (6), we can write $\alpha \propto L^4/g^5$, where L is the length of the cantilever beam, and g is the gap between the two electrodes. The maximum length of the cantilever beam, which does not collapse onto the substrate due to the intermolecular forces, is called the detachment length[16]. It is a basic design parameter for NEMSs. If the length of the beam is fixed, one can calculate the minimum gap $g_{\min}$ between the beam and the substrate to ensure that the beam does not adhere to the substrate due to the intermolecular forces. The detachment length and the minimum gap of the cantilever beam can be obtained from the critical value α^* and the second formula in Eq. (6).

Finally, we indicate that the calculation is readily amenable to the increase in the number of the integral nodes in the Gaussian quadrature rule, although the present results for 10 integral nodes are sufficiently accurate. We have checked that the results for 20 integral nodes are almost identical with the present results for 10 integral nodes. When $\alpha = 0.7, \gamma = 0.65$, and $\eta = 3$, the difference between the obtained $u_{\text{tip}}^{\text{PI}}$ for 10 nodes and 20 nodes is less than $1.117\,77 \times 10^{-12}$.

4 Conclusions

We have considered the distributed parameter model of the NEMS cantilever actuators incorporating the effects of the surface energy, the Casimir force, and the fringing field. A quartic polynomial is proposed as the shape function for the cantilever beam, and the analytic expressions for the tip deflection and pull-in parameters of the beam are derived by using the Gaussian quadrature rule. The new quartic shape function satisfies all of the four boundary values, but the quadratic shape function used in the previous investigations satisfies only three of the four boundary values. Although we have applied a numeric integral method, we derive the analytic expressions preserving the model parameters for the tip deflection and pull-in parameters of the beam. The MEMS cantilever actuators and the freestanding nano-actuators are included as two special cases in our parametric analyses. The results show that our analyses for the influence of the surface energy, the Casimir force, and the fringing field on the pull-in instability are convenient.

References

[1] Pelesko, J. A. and Bernstein, D. H. *Modeling MEMS and NEMS*, Chapman and Hall/CRC, Boca Raton (2003)

[2] Zhang, W. M., Yan, H., Peng, Z. K., and Meng, G. Electrostatic pull-in instability in MEMS/NEMS: a review. *Sensors and Actuators, A: Physical*, **214**, 187–218 (2014)

[3] Kuang, J. H. and Chen, C. J. Adomian decomposition method used for solving non-linear pull-in behavior in electrostatic micro-actuators. *Mathematical and Computer Modelling*, **41**, 1479–1491 (2005)

[4] Lin, W. H. and Zhao, Y. P. Pull-in instability of micro-switch actuators: model review. *International Journal of Nonlinear Sciences and Numerical Simulation*, **9**, 175–183 (2008)

[5] Koochi, A., Kazemi, A. S., Beni, Y. T., Yekrangi, A., and Abadyan, M. Theoretical study of the effect of Casimir attraction on the pull-in behavior of beam-type NEMS using modified Adomian method. *Physica E: Low-dimensional Systems and Nanostructures*, **43**, 625–632 (2010)

[6] Ramezani, A., Alasty, A., and Akbari, J. Closed-form solutions of the pull-in instability in nano-cantilevers under electrostatic and intermolecular surface forces. *International Journal of Solids and Structures*, **44**, 4925–4941 (2007)

[7] Lin, W. H. and Zhao, Y. P. Non-linear behavior for nano-scale electrostatic actuators with Casimir force. *Chaos, Solitons and Fractals*, **23**, 1777–1785 (2005)

[8] Koochi, A. and Abadyan, M. Efficiency of modified Adomian decomposition for simulating the instability of nano-electromechanical switches: comparison with the conventional decomposition method. *Trends in Applied Sciences Research*, **7**, 57–67 (2012)

[9] Abadyan, M. R., Beni, Y. T., and Noghrehabadi, A. Investigation of elastic boundary condition on the pull-in instability of beam-type NEMS under van der Waals attraction. *Procedia Engineering*, **10**, 1724–1729 (2011)

[10] Soroush, R., Koochi, A., Kazemi, A. S., Noghrehabadi, A., Haddadpour, H., and Abadyan, M. Investigating the effect of Casimir and van der Waals attractions on the electrostatic pull-in instability of nano-actuators. *Physica Scripta*, **82**, 045801 (2010)

[11] Salekdeh, A. Y., Koochi, A., Beni, Y. T., and Abadyan, M. Modeling effects of three nano-scale physical phenomena on instability voltage of multi-layer MEMS/NEMS: material size dependency, van der Waals force and non-classic support conditions. *Trends in Applied Sciences Research*, **7**, 1–17 (2012)

[12] Beni, Y. T., Koochi, A., and Abadyan, M. Theoretical study of the effect of Casimir force, elastic boundary conditions and size dependency on the pull-in instability of beam-type NEMS. *Physica E: Low-dimensional Systems and Nanostructures*, **43**, 979–988 (2011)

[13] Koochi, A., Kazemi, A., Khandani, F., and Abadyan, M. Influence of surface effects on size-dependent instability of nano-actuators in the presence of quantum vacuum fluctuations. *Physica Scripta*, **85**, 035804 (2012)

[14] Noghrehabadi, A., Ghalambaz, M., and Ghanbarzadeh, A. A new approach to the electrostatic pull-in instability of nano-cantilever actuators using the ADM-Padé technique. *Computers and Mathematics with Applications*, **64**, 2806–2815 (2012)

[15] Ramezani, A., Alasty, A., and Akbari, J. Closed-form approximation and numerical validation of the influence of van der Waals force on electrostatic cantilevers at nano-scale separations. *Nanotechnology*, **19**, 015501 (2008)

[16] Lin, W. H. and Zhao, Y. P. Dynamic behavior of nano-scale electrostatic actuators. *Chinese Physics Letters*, **20**, 2070–2073 (2003)

[17] Ma, J. B., Jiang, L., and Asokanthan, S. F. Influence of surface effects on the pull-in instability of NEMS electrostatic switches. *Nanotechnology*, **21**, 505708 (2010)

[18] Duan, J. S. and Rach, R. A pull-in parameter analysis for the cantilever NEMS actuator model including surface energy, fringing field and Casimir effects. *International Journal of Solids and Structures*, **50**, 3511–3518 (2013)

[19] Israelachvili, J. N. *Intermolecular and Surface Forces*, Academic Press, London (1992)

[20] Mostepanenko, V. M. and Trunov, N. N. *The Casimir Effect and Its Application*, Oxford Science Publications, New York (1997)

[21] Lamoreaux, S. K. The Casimir force: background, experiments, and applications. *Reports on Progress in Physics*, **68**, 201–236 (2005)

[22] Rodriguez, A. W., Capasso, F., and Johnson, S. G. The Casimir effect in microstructured geometries. *Nature Photonics*, **5**, 211–221 (2011)

[23] Guo, J. G. and Zhao, Y. P. Dynamic stability of electrostatic torsional actuators with van der Waals effect. *International Journal of Solids and Structures*, **43**, 675–685 (2006)

[24] Guo, J. G. and Zhao, Y. P. Influence of van der Waals and Casimir forces on electrostatic torsional actuators. *Journal of Microelectromechanical Systems*, **13**, 1027–1035 (2004)

[25] Lin, W. H. and Zhao, Y. P. Stability and bifurcation behaviour of electrostatic torsional NEMS varactor influenced by dispersion forces. *Journal of Physics*, *D*: *Applied Physics*, **40**, 1649–1654 (2007)

[26] Duan, J. S., Rach, R., and Wazwaz, A. M. Solution of the model of beam-type micro- and nano-scale electrostatic actuators by a new modified Adomian decomposition method for non-linear boundary value problems. *International Journal of Non-Linear Mechanics*, **49**, 159–169 (2013)

[27] Gurtin, M. E. and Murdoch, A. I. A continuum theory of elastic material surfaces. *Archive for Rational Mechanics and Analysis*, **57**, 291–323 (1975)

[28] He, J. and Lilley, C. M. Surface effect on the elastic behavior of static bending nano-wires. *Nano Letters*, **8**, 1798–1802 (2008)

[29] Wang, G. F. and Feng, X. Q. Surface effects on buckling of nano-wires under uniaxial compression. *Applied Physics Letters*, **94**, 141913 (2009)

[30] Fu, Y. and Zhang, J. Size-dependent pull-in phenomena in electrically actuated nano-beams incorporating surface energies. *Applied Mathematical Modelling*, **35**, 941–951 (2011)

[31] Miller, R. E. and Shenoy, V. B. Size-dependent elastic properties of nano-sized structural elements. *Nanotechnology*, **11**, 139–147 (2000)

[32] Jiang, L. Y. and Yan, Z. Timoshenko beam model for static bending of nano-wires with surface effects. *Physica E*: *Low-dimensional Systems and Nanostructures*, **42**, 2274–2279 (2010)

[33] Gupta, R. K. *Electrostatic Pull-in Test Structure Design for In-situ Mechanical Property Measurements of Microelectromechanical Systems* (*MEMS*), Ph. D. dissertation, Massachusetts Institute of Technology, Cambridge (1997)

[34] Huang, J. M., Liew, K. M., Wong, C. H., Rajendran, S., Tan, M. J., and Liu, A. Q. Mechanical design and optimization of capacitive micromachined switch. *Sensors Actuators*, *A*: *Physical*, **93**, 273–285 (2001)

[35] Duan, J. S. and Rach, R. A new modification of the Adomian decomposition method for solving boundary value problems for higher order non-linear differential equations. *Applied Mathematics and Computation*, **218**, 4090–4118 (2011)

[36] Petersen, K. E. Dynamic micromechanics on silicon: techniques and devices. *IEEE Transaction on Electron Devices*, **25**, 1241–1250 (1978)

[37] Ke, C. H., Pugno, N., Peng, B., and Espinosa, H. D. Experiments and modeling of carbon nanotube-based NEMS devices. *Journal of the Mechanics and Physics of Solids*, **53**, 1314–1333 (2005)

[38] Abramowitz, M. and Stegun, I. A. *Handbook of Mathematical Functions with Formulas, Graphs, and Mathematical Tables*, Dover, New York (1972)

Appendix A Synopsis of Gaussian quadrature rule

An n-node Gaussian quadrature rule is

$$\int_{-1}^{1} f(z)\mathrm{d}z \approx \sum_{i=1}^{n} w_i f(z_i),$$

where z_i are the Gaussian nodes, and ω_i are the weights. The Gaussian quadrature rule has the highest algebraic accuracy $2n-1$, i.e., the integral rule exactly holds for polynomial functions of the degree no more than $2n-1$.

The nodes and the weights can be readily calculated as follows.

The ith Gaussian node z_i is the ith zero of the Legendre polynomials $L_n(z)$. Its weight can be given by[38]

$$w_i = \frac{2}{(1-z_i^2)(L_n'(z_i))^2}.$$

The Legendre polynomials $L_n(z)$ satisfy the recursion relations as follows:

$$\begin{cases} L_0(z) = 1, \quad L_1(z) = z, \\ L_{n+1}(z) = \dfrac{(2n+1)z}{n+1} L_n(z) - \dfrac{n}{n+1} L_{n-1}(z), \quad n \geqslant 1. \end{cases}$$

We note that the built-in command "Legendre $P[n, z]$" in MATHEMATICA can conveniently generate the Legendre polynomials $L_n(z)$.

In Table 4, we list the nodes and the weights for the n-node Gaussian quadrature rule for $n = 2$ through $n = 5$ and $n = 10$.

Table 4 Nodes and weights for Gaussian quadrature rule

Number of nodes, n	Node, z_i	Weight, ω_i
2	±0.577 350 26	1.000 000 00
3	0.000 000 00	0.888 888 89
	±0.774 596 66	0.555 555 56
4	±0.339 981 04	0.652 145 15
	±0.861 136 31	0.347 854 85
5	0.000 000 00	0.568 888 89
	±0.538 469 31	0.478 628 67
	±0.906 179 85	0.236 926 89
10	±0.148 874 34	0.295 524 22
	±0.433 395 39	0.269 266 72
	±0.679 409 57	0.219 086 36
	±0.865 063 37	0.149 451 35
	±0.973 906 53	0.066 671 34